We are IntechOpen,
the world's leading publisher of
Open Access books
Built by scientists, for scientists

6,900
Open access books available

186,000
International authors and editors

200M
Downloads

154
Countries delivered to

Our authors are among the
TOP 1%
most cited scientists

12.2%
Contributors from top 500 universities

Selection of our books indexed in the Book Citation Index
in Web of Science™ Core Collection (BKCI)

Interested in publishing with us?
Contact book.department@intechopen.com

Numbers displayed above are based on latest data collected.
For more information visit www.intechopen.com

4

Reaction-Diffusion Algorithm for Vision Systems

Atsushi Nomura*, Makoto Ichikawa**, Rismon H. Sianipar*, and
Hidetoshi Miike*
*Yamaguchi University, **Chiba University*
Japan

1. Introduction

Vision systems require fundamental algorithms of image processing and vision computing. Algorithms of edge detection, grouping and stereo disparity detection are typical examples. Marr and his collaborators proposed several effective algorithms of edge detection and stereo disparity detection, in particular, in a computational approach (Marr, 1982).

Marr and Hildreth had previously proposed an edge detection algorithm (Marr and Hildreth, 1980), in which edge points were defined as those having a high brightness gradient over space. They utilized the Gaussian filter combined with the Laplacian one; the Gaussian filter removes noise components, and the Laplacian filter senses a brightness gradient. They additionally proposed an alternative algorithm that utilizes difference of two Gaussian filters having two different space constants of excitation and inhibition. Both of these two algorithms utilize the Gaussian filter; the output of the filter is equivalent to the solution of the diffusion equation. Their proposal highly attracted other researchers' attention, resulting in the development of many edge detection algorithms starting from the Gaussian filter or the diffusion equation, in which, for example, anisotropy was introduced into the diffusion equation (Perona & Malik, 1990).

Regarding stereo disparity detection, Marr and Poggio proposed "the cooperative algorithm" (Marr and Poggio, 1976; Marr et al., 1978). Stereo cameras project a target point located in a three-dimensional world onto two points on their left and right image planes; stereo disparity refers to the difference of the two points. A stereo disparity map helps to reconstruct the three-dimensional world and thus has many applications in vision systems. To construct a reliable stereo disparity map, Marr and Poggio made two important constraints, one of which is that spatial adjacent points on a stereo disparity map must have similar disparity levels. This constraint allows us to propagate disparity information in a spatial local area. Therefore, the cooperative algorithm for the stereo disparity detection utilizes an information propagation mechanism, which roughly refers to the mechanism of diffusion. Using this cooperative algorithm, other researchers have proposed several methods of stereo disparity detection (Zitnick & Kanade, 2000).

There are several interesting approaches to image processing and vision computing not only in the field of computer science, but also in the natural sciences. Kuhnert et al. demonstrated that a chemical reaction system solves the typical image processing tasks of edge detection

and segmentation (Kuhnert, 1986; Kuhnert et al., 1989). The mathematical model of the chemical reaction system cited in their demonstration is a type of reaction-diffusion system, which consists of non-linear reaction terms combined with diffusion equations. Their successful demonstration showing the capability of the reaction-diffusion system to process images strongly motivated us to further develop our image processing and vision computing algorithms by incorporating the reaction-diffusion system. In addition, Asai and his collaborators have been proposing reaction-diffusion devices for image processing (Asai et al., 2005; Adamatzkey et al., 2005). They realized their algorithms by utilizing large-scale integrated circuits and applied them to realistic applications. Reaction-diffusion systems can be found in a variety of natural systems (Murray, 1989). The FitzHugh-Nagumo equations are typical reaction-diffusion equations; they simulate an information transmission phenomenon along a nerve axon (FitzHugh, 1961; Nagumo et al., 1962).

This chapter presents a class of algorithms for typical image processing and vision computing such as edge detection, grouping and stereo disparity detection, all of which are fundamental functions needed for vision systems. The algorithms utilize reaction-diffusion equations, so we call this class of algorithms "reaction-diffusion algorithms". In particular, we utilize the FitzHugh-Nagumo type reaction-diffusion equations, since we are interested in biological systems and also in the human early visual processing mechanism. Previous algorithms, such as those proposed by Marr et al., utilize the Gaussian filter or a diffusion equation. In contrast to those algorithms, our reaction-diffusion algorithm utilizes two diffusion equations coupled with non-linear reaction terms. Under a certain ratio of the two diffusion coefficients, the non-linear reaction terms play an important role in solving the problem of unexpected blurring caused by simple diffusion-based algorithms.

2. Reaction-Diffusion System

The reaction-diffusion system with the two variables (u,v) consists of

$$\partial_t u = D_u \nabla^2 u + f(u,v) , \quad \partial_t v = D_v \nabla^2 v + g(u,v) . \tag{1}$$

The operator ∂_t denotes the temporal partial derivative $\partial/\partial t$. The Laplacian operator ∇^2 denotes $\partial^2/\partial x^2 + \partial^2/\partial y^2$ in the two-dimensional coordinate system of (x,y); D_u is the diffusion coefficient of the variable u and D_v is that of v. The functions $f(u,v)$ and $g(u,v)$ are reaction terms, which depend on particular phenomena. The reaction terms of the FitzHugh-Nagumo equations (FitzHugh, 1961; Nagumo et al., 1962) are

$$f(u,v) = \frac{1}{\varepsilon}\left[u(u-a)(1-u)-v\right], \; g(u,v) = u - bv , \tag{2}$$

where a and b are constants and ε is a positive small constant ($0<\varepsilon<<1$).

Let us focus on the set of the ordinary differential equations $du/dt=[u(u-a)(1-u)-v]/\varepsilon$ and $dv/dt=u-bv$ in order to understand the basic behaviour of the FitzHugh-Nagumo equations. The set of the equations has two different types of system behaviour, the mono-stable system and the bi-stable one, depending on the parameter values of a and b. For example, when $a=0.25$ and $b=1.0$, the system becomes mono-stable. In this case, any solution starting from any point on a phase plot finally converges to the stable point A, as time proceeds [see Figs. 1(a) and 1(b)]. When $a=0.25$ and $b=10$, solutions converge to either of the two stable points A or C, and that is the bi-stable system [see Figs. 1(a) and 1(c)]. The variable u is an

activator, and the variable v is an inhibitor. When $u>a$ and $v=0$ at an initial state, because of $du/dt>0$, the variable u increases spontaneously; this is the self-activation process. After u reaches 1.0, the variable v also begins to increase. The increasing process of the variable v inhibits the variable u from increasing; this is the self-inhibition process. When $u<a$ at an initial state, a solution directory converges to the stable point A. When starting from the initial condition of $v=0$, the system works as a time-dependent threshold function, in which the parameter a is its threshold value. Therefore, a set of solutions (u,v) traces a trajectory indicated by arrows in the mono-stable system. In the bi-stable system, a set of solutions starting from $u>a$ and $v=0$ remains at the stable equilibrium point C.

Let us return to the full reaction-diffusion system. When the two diffusion coefficients of the activator variable u and the inhibitor variable v are in the condition of $D_u>D_v$, the reaction-diffusion system self-organizes the temporally evolving spatial pattern which propagates in space. However, when the two diffusion coefficients are in the condition of $D_u<<D_v$, the system self-organizes a static pattern (Turing, 1952; Kondo & Asai, 1995). By choosing appropriate parameter values and finite differences for the discrete version of the FitzHugh-Nagumo type reaction-diffusion equations under $D_u<<D_v$, we obtain spatial static patterns (Ebihara et al., 2003a; Nomura et al., 2003). Figure 2 shows numerical results obtained by the reaction-diffusion system of Eqs. (1) and (2), in which an initial condition for u has the binary digit of 0 or 1 randomly distributed in the centre part of the one-dimensional space x. The mono-stable system self-organizes the two impulses standing at the edge points; that is, the impulses divide the one-dimensional space into the centre part and the remaining flat parts. The bi-stable system also divides the space into such parts. These results show that the reaction-diffusion system has the ability to detect edge points and segments from the binary data. Note that the spatial distributions shown in Figs. 2(b) and 2(c) are not transient but almost static.
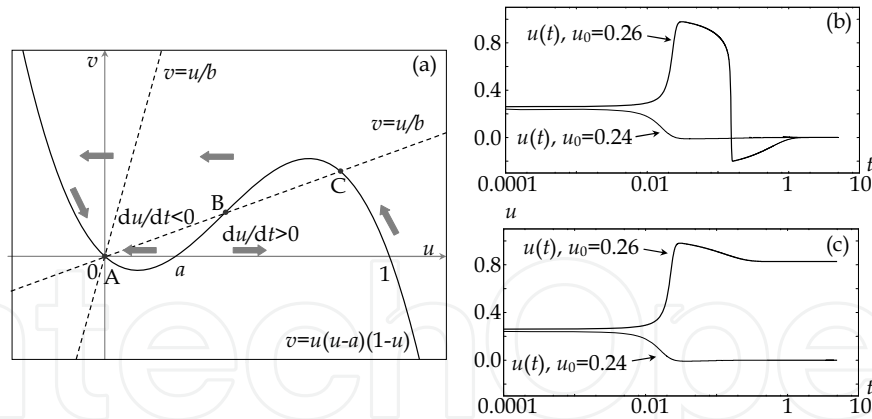

Figure 1. System behaviour of the FitzHugh-Nagumo equations $du/dt=[u(u-a)(1-u)-v]/\varepsilon$ and $dv/dt=u-bv$. (a) Phase plot for the equations. A and C are stable equilibrium points; B is an unstable point. (b) Temporal development of $u(t)$ for the mono-stable system ($a=0.25$, $b=1.0$). (c) Temporal development of $u(t)$ for the bi-stable system ($a=0.25$, $b=10$). Both of (b) and (c) show how the solutions starting from the two different initial conditions ($u_0=0.24$ and $u_0=0.26$) temporally change; the initial condition for $v(t)$ is zero and $\varepsilon=10^{-3}$ for both.
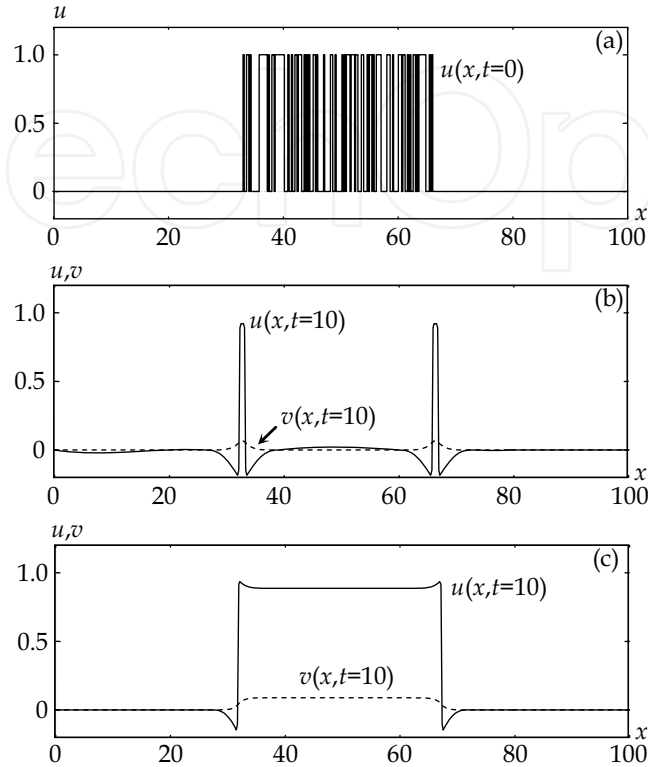
Figure 2. One-dimensional numerical results of the FitzHugh-Nagumo type reaction-diffusion equations of Eqs. (1) and (2). (a) Initial condition of $u(x,t=0)$; (b) spatial distributions of $u(x,t=10)$ and $v(x,t=10)$ for the mono-stable system with $a=0.01$ and $b=1.0$; (c) those for the bi-stable system with $a=0.01$ and $b=10$. The initial conditions for v in both (b) and (c) are $v(x,t=0)=0$. The other parameter values are $D_u=1.0$, $D_v=10$ and $\varepsilon=1.0\times10^{-3}$.

3. Previous Algorithms

Marr and his collaborators proposed algorithms for edge detection and stereo disparity detection. This section presents the previously proposed algorithms by Marr et al. and a more recently developed algorithm for stereo disparity detection.

3.1 Edge detection

Marr and Hildreth proposed an edge detection algorithm (Marr & Hildreth, 1980) in which edge points were generally defined as those having a high spatial gradient in image brightness distribution. Their algorithm consists of the following three steps to detect edge points from an image brightness distribution function denoted by $I(x)$ in the one-dimensional space x. The first step is to compute the convolution of the image function and the Gaussian function as follows:

$$G(x;\sigma) = \frac{1}{\sqrt{2\pi}\sigma} \exp\left(-\frac{x^2}{2\sigma^2}\right). \tag{3}$$

The parameter σ is the constant representing spatial spread. The convolution of the image function and the Gaussian function reduces noise contained in the image function. Natural images have noisy signals, which could produce pseudo edge points. Therefore, before detecting edge points, by applying a Gaussian filter to the image function, we obtain its smoothed function: $G*I(x)$ [see Figs. 3(a) and 3(b)], in which the symbol * denotes the convolution operator. The first-order derivative operator ∇ applied to $G*I(x)$ provides the distribution shown in Fig. 3(c). The second-order derivative operator ∇^2 for $G*I(x)$ provides the spatial distribution that is across the zero level at the edge point. That is, the zero-crossing point corresponds to the edge point. Thus, we can detect edge points by finding zero-crossing points in the distribution of $\nabla^2(G*I)$. This is the well-known edge detection algorithm that utilizes the 'Laplacian of Gaussian' (LoG) filter.

Another edge detection algorithm utilizes two Gaussian filters with different space constants. One of the filters has a small space constant denoted by σ_e, and the other has a large space constant denoted by σ_i. We can detect edge points by finding zero-crossing points in the output of the filter consisting of the difference of the two Gaussian filters (DOG). The DOG filter is expressed as
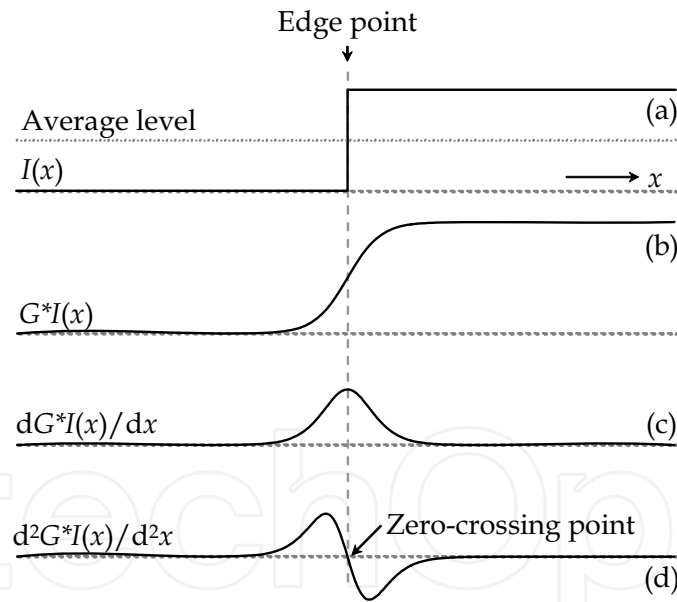

Figure 3. Edge detection algorithm proposed by Marr and Hildreth in the one-dimensional space x. (a) Image brightness distribution function $I(x)$ and its average level on brightness; (b) output of the Gaussian filter applied to $I(x)$; (c) first-order derivative of $G*I(x)$; (d) second-order derivative of $G*I(x)$. The zero-crossing point in the second derivative (d) corresponds to the edge point of the original $I(x)$.

$$\text{DOG} = G(x;\sigma_{\text{e}}) - G(x;\sigma_{\text{i}}) . \tag{4}$$

Marr and Hildreth pointed out that the constant σ_{i} is larger than σ_{e} and the optimal ratio of the two constants $(\sigma_{\text{e}}/\sigma_{\text{i}})$ is 1.6 or 1.7.

Let us consider the following simple diffusion equation having the spatial and temporal distribution function $u(x,t)$ and the diffusion coefficient D_u :

$$\partial_t u = D_u \nabla^2 u . \tag{5}$$

When the diffusion equation has the initial condition of a spatial function $u_0(x)$, the next convolution of the function $u_0(x)$ and the Gaussian function $G_t(x,t;D_u)$ becomes the solution of the diffusion equation at time t,

$$u(x,t) = u_0(x) * G_t(x,t;D_u) , \tag{6}$$

where

$$G_t(x,t;D_u) = \frac{1}{2\sqrt{\pi D_u t}} \exp\left(-\frac{x^2}{4D_u t}\right) . \tag{7}$$

Therefore, when the diffusion equation has the initial condition of an image function $I(x)$, it provides the solution equivalent to the Gaussian filter output for the image function. If an image pool stores the solution $u(x,t)$ of the diffusion equation during a short time Δt, edge points are detected from zero-crossing points in $[u(x,t-\Delta t)-u(x,t)]$ (Sunayama et al., 2000) derived from the simple diffusion equation of Eq. (5), since the space constant of the Gaussian function described in Eq. (7) depends on time t. Another algorithm for edge detection utilizes the next two simple diffusion equations having the two variables (u,v) and the initial conditions of $u(x,t=0)=v(x,t=0)=I(x)$. Under the condition of $D_u<D_v$, zero-crossing points in the difference distribution $(u-v)$ correspond to edge points.

$$\partial_t u = D_u \nabla^2 u , \quad \partial_t v = D_v \nabla^2 v \tag{8}$$

3.2 Stereo disparity detection

Figure 4 shows the arrangement of stereo cameras and an object in a three-dimensional world, and a basic idea for stereo disparity detection. The left camera projects the object point onto a position (x_L,y) on its image plane $I_L(x,y)$; the right one does it onto (x_R,y) on $I_R(x,y)$. The difference between the two positions is the stereo disparity $d=x_L-x_R$, which can be used to obtain the depth of the object (Gonzalez & Woods, 1992). If we can find the correspondence between the two points (x_R,y) and (x_L,y) from only the two image brightness distribution functions $I_L(x,y)$ and $I_R(x,y)$, we can obtain the stereo disparity, that is, the depth of the object point. To find the stereo correspondence, we overlap the two image distributions $I_L(x,y)$ and $I_R(x,y)$ at every possible disparity level d in $\Psi_d=\{d_0,d_1,\ldots,d_{N-1}\}$, in which N denotes the number of possible disparity levels. If the object has a disparity level d, a cross-correlation map $C_d(x,y)$ computed for $I_L(x,y)$ and $I_R(x+d,y)$ has a high correlation value nearly equal to 1.0 at the object position. By finding the highest value of $C_d(x,y)$ for all of the possible disparity levels, we can obtain a disparity map.
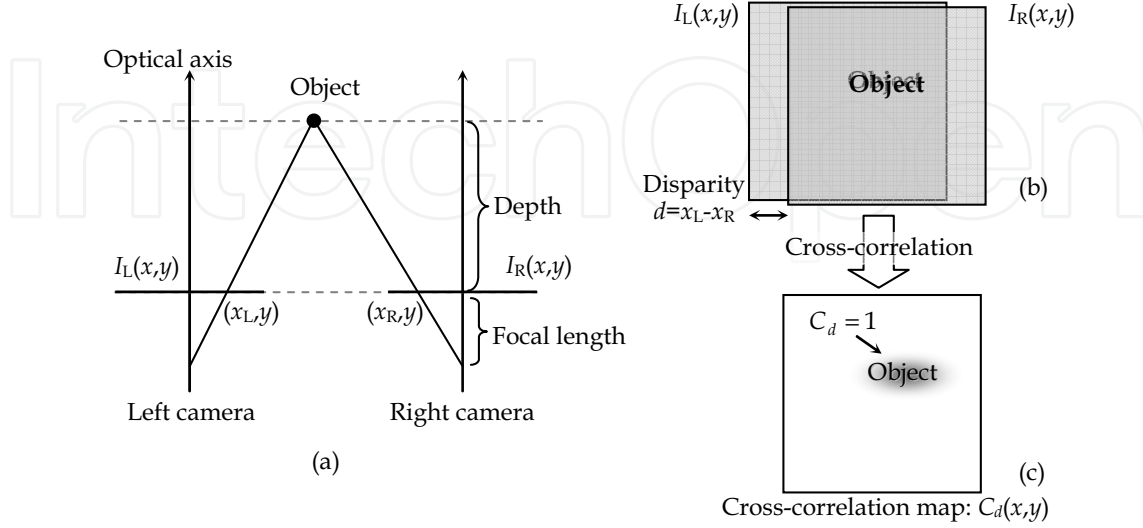
Figure 4. Stereo vision geometry and a cross-correlation map. (a) Stereo cameras and an object in a three-dimensional world. An object point is projected onto the image plane $I_L(x,y)$ of the left camera and onto the image plane $I_R(x,y)$ of the right one. (b) Stereo images overlapped with a stereo disparity level d. (c) Cross-correlation map $C_d(x,y)$ obtained between the stereo images with a disparity level d. When $d=x_L-x_R$, C_d becomes 1.

Following the above idea of detecting a stereo disparity map, we first compute a cross-correlation map $C_d(x,y)$ between stereo images. For a binary stereo image pair such as the random-dot stereograms (Julesz, 1960), a simple logic operation provides the cross-correlation map as

$$C_d(x,y) = \neg[I_L(x,y) \oplus I_R(x+d,y)], \qquad (9)$$

where $\neg[\cdot \oplus \cdot]$ is the XNOR logic operation that gives 1 for a matched pair and 0 for an unmatched one (Nomura et al., 1999). For real stereo images, the normalized cross-correlation function computed in a spatial local area L_S,

$$C_d(x,y) = \frac{1}{\max\{s_L, s_R\}} \sum_{(x',y') \in L_S} \left[I_L(x+x', y+y') - \overline{I_L(x,y)} \right] \times \left[I_R(x+x'+d, y+y') - \overline{I_R(x+d,y)} \right] \quad (10)$$

provides similarity between the stereo images, where s_L denotes the standard deviation of I_L in L_S surrounding the point (x,y) and s_R denotes the standard deviation of I_R in L_S surrounding $(x+d,y)$; $\overline{I_L}$ and $\overline{I_R}$ are the averages of I_L and I_R in L_S as shown in

$$s(x,y) = \left\{ \frac{1}{N_{L_S}} \sum_{(x',y') \in L_S} \left[I(x+x', y+y') - \overline{I(x,y)} \right]^2 \right\}^{1/2}, \quad \overline{I(x,y)} = \frac{1}{N_{L_S}} \sum_{(x',y') \in L_S} I(x+x', y+y'), \quad (11)$$

where N_{L_S} is the number of points in L_S. The cross-correlation map $C_d(x,y)$ is provided for use in the next main step of stereo disparity detection. Several stereo algorithms utilize other

types of similarity measures such as the sum of absolute differences (SAD) between stereo images (Brown et al., 2003).

It is difficult to solve the stereo correspondence problem using only the cross-correlation map. The cross-correlation value C_d becomes 1 for a matched pair between stereo images. However, in real situations, images have many similar brightness patterns, which cause many miss matched pairs in $C_d(x,y)$. Therefore, there is much uncertainty in finding correct match pairs in the cross-correlation map. To solve the uncertainty and detect a reliable stereo disparity map, we need additional information or constraint, as described next.

Marr and Poggio proposed a cooperative stereo algorithm. They imposed two important constraints on stereo disparity distribution, a continuity constraint and a uniqueness constraint. The continuity constraint states that the stereo disparity distribution varies smoothly over a stereo disparity map or in a local spatial area called "local support". This is generally true except for object boundaries. The other uniqueness constraint states that a point on a stereo disparity map has only one disparity level. This is also true except for a transparent object. According to these two constraints and the biologically motivated idea of a cell network, they formulated the next update function for the cell state $S_d^t(x,y)$ of the disparity level d and the position (x,y) at the t-th iteration step, as follows:

$$S_d^{t+1}(x,y) = \sigma\left(\sum_{(x',y',d')\in\Omega_e} S_{d+d'}^t(x+x',y+y') - \lambda \sum_{(x',y',d')\in\Omega_i(x,y,d)} S_{d'}^t(x',y') + C_d(x,y), T \right). \tag{12}$$

In Eq. (12), $\sigma(S,T)$ denotes the threshold function, in which the parameter T is the threshold value for S. When $S<T$, $\sigma(S,T)$ provides zero; when $S\geq T$, it provides 1. The symbol Ω_e denotes the spatial local support area for the continuity constraint, and Ω_i denotes the inhibition area for the uniqueness constraint [see Fig. 1 in the article (Zitnick and Kanade, 2000)]. The parameter λ is a positive inhibition constant. After iterations needed for convergence of the update function of Eq. (12), we obtain the disparity map $M(x,y,t)$ at the t-th step by finding the maximum value of $S_d^t(x,y)$ for all of the possible disparity levels at a particular position (x,y),

$$M(x,y,t) = \arg\max_{d\in\Psi_d} S_d^t(x,y). \tag{13}$$

The original cooperative algorithm works well for random-dot stereograms. However, the algorithm does not work for real stereo images.

Zitnick and Kanade improved the cooperative algorithm (Zitnick & Kanade, 2000). Their algorithm achieves good performance not only for random-dot stereograms but also for real stereo images, compared with the original cooperative algorithm. In addition, their algorithm can detect an occlusion area, which was not taken into account by the original cooperative algorithm. The update function proposed by Zitnick and Kanade is

$$S_d^{t+1}(x,y) = C_d(x,y) \times \left[\frac{R_d^t(x,y)}{\sum_{(x'',y'',d'')\in\Omega_i(x,y,d)} R_{d''}^t(x'',y'')} \right]^\alpha, \tag{14}$$

where α is a constant for convergence of the update function, and R_d^t is

$$R_d^t(x,y) = \sum_{(x',y',d') \in \Omega_e} S_{d+d'}^t(x+x', y+y') . \qquad (15)$$

The algorithm finally detects the disparity map, including the occlusion area, by

$$M(x,y,t) = \begin{cases} \arg\max_{d \in \Psi_d} S_d^t(x,y) & \text{if} \quad \max_{d \in \Psi_d} S_d^t \geq T, \\ d_\infty & \text{otherwise.} \end{cases} \qquad (16)$$

If the maximum value of S_d^t at the point (x,y) is less than T, the algorithm classifies the point (x,y) as the occlusion denoted by d_∞. The threshold value $T \leq 0$ switches off the algorithm of the occlusion area detection.

4. Reaction-Diffusion Algorithm

This section presents the reaction-diffusion algorithm for edge detection, grouping and stereo disparity detection by means of the FitzHugh-Nagumo type reaction-diffusion system presented in section 2. The reaction-diffusion system consists of partial-differential equations; thus, this section additionally presents numerical schemes required for the computation of the equations.

4.1 Edge detection
The one-dimensional numerical result of Fig. 2(b) lets us recognize that the FitzHugh-Nagumo type reaction-diffusion system has the ability of edge detection. It self-organizes impulses at edge points, if the initial condition is binary data. To utilize the edge detection algorithm on multi-valued image, we modify the FitzHugh-Nagumo equations. Let us recall the situation of Fig. 3 showing the original image brightness distribution $I(x,y)$ and its average brightness level. The image brightness distribution $I(x,y)$ is across its average level at the edge position. In Eq. (2), the parameter value a is the threshold value for the initial condition, as stated in the description for the ordinary differential equation and also as shown in Fig. 1. Therefore, when substituting the average level of $I(x,y)$ for the parameter value a of the FitzHugh-Nagumo equations, we can expect to realize the edge detection function. A simple diffusion equation provides a local average value of an initial condition and its local area is spreading as time proceeds. Thus, we estimate the average level or the threshold level of a with an additional diffusion equation starting from the initial condition of $I(x,y)$. The overall set of equations for edge detection in the reaction-diffusion algorithm is the following:

$$\partial_t u = D_u \nabla^2 u + f(u,v,a) , \quad \partial_t v = D_v \nabla^2 v + g(u,v) , \quad \partial_t a = D_a \nabla^2 a , \qquad (17)$$

$$f(u,v,a) = \frac{1}{\varepsilon}[u(u-a)(1-u)-v], \quad g(u,v) = u - bv . \qquad (18)$$

Note that Eq. (17) handles the parameter a as a spatial and temporal variable $a=a(x,y,t)$, as opposed to the constant parameter a of the original FitzHugh-Nagumo equations. The

diffusion coefficients D_u, D_v and D_a should satisfy the relation $D_u \ll D_v \ll D_a$. The Turing-like condition $D_u \ll D_v$ is from section 2, and the condition $D_v \ll D_a$ is for the computation of the local average level. Initial conditions for (u,v,a) are given as

$$u(x,y,t=0) = a(x,y,t=0) = a_0 \times I(x,y), \; v(x,y,t=0) = 0, \tag{19}$$

where $I(x,y)$ is a normalized image brightness distribution ranging from 0 to 1; a_0 is a constant. The Neumann boundary condition governs the four sides of the rectangular image region of u, v and a such as

$$\partial_x u\big|_{\text{Left,Right}} = 0, \; \partial_y u\big|_{\text{Top,Bottom}} = 0. \tag{20}$$

4.2 Grouping

The human vision system has a grouping mechanism for processing visual stimuli. For example, when the system is exposed to the visual stimulus of an image that consists of several different features such as orientation, it will perceive several groups corresponding to particular orientation features (Beck, 1966). That is, for example, the human vision system can reconstruct the group map of Fig. 5(a) from the visual stimulus of Fig. 5(b). This is the grouping mechanism. We believe that the grouping mechanism underlies several human visual functions such as stereo disparity detection.

In accordance with the reaction-diffusion algorithm, we present a model that can reconstruct a grouping map from a visual stimulus. Figure 6 shows the overall flow diagram of visual processing for the grouping mechanism (Nomura et al., 2004). During the first stage, several orientation-selective filters detect the orientation feature distributions $s_n(x,y)$ from the input image $I(x,y)$ of a visual stimulus. For example, Fig. 7 shows the outputs s_n (n=0,1,2) of the three different orientation-selective filters applied to the input image of Fig. 5(b). Then, during the next stage, the distributions $s_n(x,y)$ are fed to the multi-sets of reaction-diffusion equations; each set has the two variables (u_n,v_n) and is slightly modified from the original FitzHugh-Nagumo equations. As time proceeds, the multi-sets of equations spontaneously self-organize groups of orientation features. Finally, the algorithm reconstructs a group map from the solutions u_n. Note that the multi-sets of the reaction-diffusion equations are mutually and inhibitedly linked through the activator variables u_n.
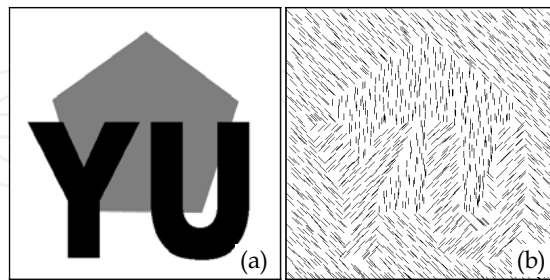

Figure 5. Group map and visual stimulus for the explanation of the grouping mechanism in the human vision system. (a) Original group map with three groups. (b) Visual stimulus having the three different features of line orientation. The image size is 400×400 pixels.
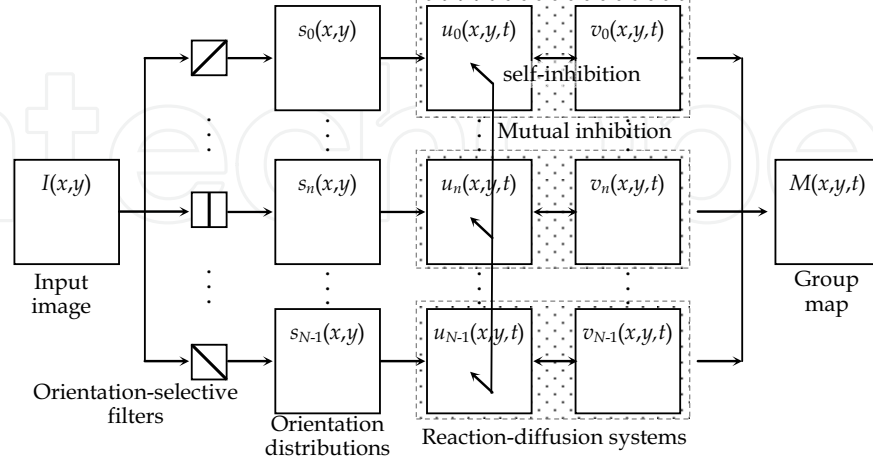
Figure 6. Flow diagram of the grouping mechanism. From the input image $I(x,y)$, orientation-selective filters provide feature distributions $s_n(x,y)$ for $n \in \{0,1,\ldots,N\text{-}1\}$, in which N denotes the number of groups. The distributions are fed to the multi-sets of the reaction-diffusion equations having the two variables (u_n, v_n). Integration of u_n provides a group map $M(x,y,t)$.

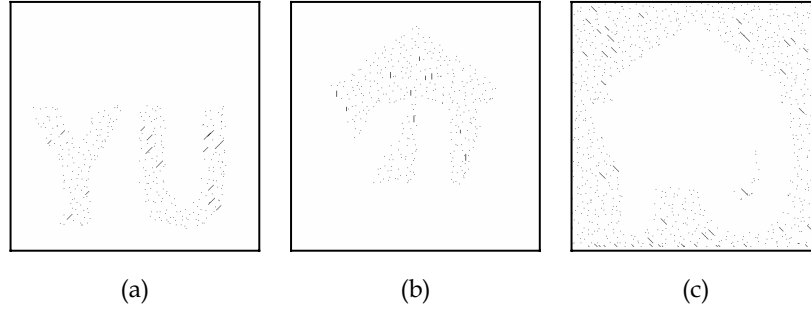(a)   (b)   (c)

Figure 7. Outputs of three orientation-selection filters. Black dots indicate the existence of orientation features of (a) $\pi/4$, (b) $2\pi/4$ and (c) $3\pi/4$. The filters are realized with a matching procedure between an input image and a template pattern of an oriented short line.

To model the grouping mechanism we must consider two important constraints. One of them is that a particular point on an image is a member of only one group and is not classified into two or more groups; that is the uniqueness constraint. The other constraint is that spatial adjacent points are likely to be members of the same group; that is the continuity constraint. A particular point except for boundary areas of groups should satisfy these two constraints. By recalling that the parameter a is the threshold value, we formulate the set of equations governing the n-th group as follows:

$$\partial_t u_n = D_u \nabla^2 u_n + f(u_n, v_n, U_n) + \mu s_n , \quad \partial_t v_n = D_v \nabla^2 v_n + g(u_n, v_n) , \tag{21}$$

$$f(u_n, v_n, U_n) = \frac{1}{\varepsilon}[u_n(u_n - a(U_n))(1 - u_n) - v_n] , \quad g(u_n, v_n) = u_n - b v_n , \tag{22}$$

where μ is a constant. The original reaction term $f(u,v)$ has a constant parameter a. In contrast to this, the modified version of the reaction term in Eq. (22) depends on the state of another set U_n, as follows:

$$a(U_n) = a_0 + U_n, \; U_n = \max_{n' \in \{0,1,\cdots,n-1,n+1,\cdots,N-1\}} u_{n'}(x,y,t), \qquad (23)$$

where a_0 is a constant and N is the number of groups. Let us consider the situation in which the variable $u_{n'}(x,y)$ of the n'-th group becomes large. This represents that the point (x,y) is already classified as the n'-th group. In that case, the n-th set must be inhibited to have a high value of u_n. Equation (23) works as the mutual inhibition mechanism by increasing the threshold value of other sets, and the multi-sets of equations exclusively become the excited state having the high value of u_n. Thus, Eq. (23) realizes the uniqueness constraint. The continuity constraint is built into the reaction-diffusion system, since the system originally has the spatial information propagation effect for its adjacent area. After convergence, the final step is to reconstruct a group map $M(x,y,t)$ by finding the maximum value of u_n at a particular point at time t as follows:

$$M(x,y,t) = \underset{n \in \{0,1,\cdots,N-1\}}{\arg\max} \; u_n(x,y,t) . \qquad (24)$$

4.3 Stereo disparity detection

The previous cooperative algorithm proposed by Marr and Poggio has the uniqueness constraint and the continuity constraint, both of which are very similar to the constraints made by the reaction-diffusion algorithm modelling the grouping mechanism. Thus, we can expect that the reaction-diffusion algorithm described with Eqs. (21) and (22) is also applicable to the stereo disparity detection; a cross-correlation map $C_d(x,y)$ obtained by Eq. (9) or Eq. (10) substitutes for $s_n(x,y)$ in Eq. (21), and the disparity level d corresponds to the number n (Nomura et al., 2005). The local support area in the stereo disparity detection is not only over space but also across the disparity direction, as proposed by Zitnick and Kanade. Thus, it is necessary to modify the function $a(U_d)$ in Eq. (23) representing the uniqueness constraint, by taking into account the distance between the current disparity level d and the level having the largest value of $u_{d'}$ in the inhibition area Ω_i. One possible formulation having the two constants of a_0 and a_1, and the switching function $\tanh(\cdot)$ is

$$a(U_d) = a_0 + U_d \times \frac{1}{2}\left[1 + \tanh(|d| - a_1)\right], \; U_d = \max_{(x',y',d') \in \Omega_i} u_{d'}(x',y',t), \; |d| = \left| d - \underset{(x',y',d') \in \Omega_i}{\arg\max} u_{d'}(x',y',t) \right|. \quad (25)$$

Finally, Eq. (24) provides a stereo disparity map $M(x,y,t)$, in the same manner.

4.4 Numerical computation for reaction-diffusion equations

The realization of the reaction-diffusion algorithm on a computer system requires numerical computation of partial differential equations. The finite difference method is applicable to the computation. For example, the partial derivatives $\partial_t u$, $\partial_x u$ and $\partial_y u$ at (x,y,t) are approximately evaluated with the finite differences of δt, δx and δy in time and two-dimensional space as

$$\partial_t u(x,y,t) \cong \frac{u_{i,j}^{k+1} - u_{i,j}^k}{\delta t}, \tag{26}$$

$$\partial_x u(x,y,t) \cong h\frac{u_{i+1,j}^{k+1} - 2u_{i,j}^{k+1} + u_{i-1,j}^{k+1}}{\delta x^2} + (1-h)\frac{u_{i+1,j}^k - 2u_{i,j}^k + u_{i-1,j}^k}{\delta x^2}, \tag{27}$$

$$\partial_y u(x,y,t) \cong h\frac{u_{i,j+1}^{k+1} - 2u_{i,j}^{k+1} + u_{i,j-1}^{k+1}}{\delta y^2} + (1-h)\frac{u_{i,j+1}^k - 2u_{i,j}^k + u_{i,j-1}^k}{\delta y^2}, \tag{28}$$

where $u_{i,j}^k$ denotes $u(i\delta x, j\delta y, k\delta t)$ in the discrete coordinate system. The first terms on the right side of Eqs. (27) and (28) are the implicit terms evaluated at (k+1), and the second terms are the explicit terms evaluated at k. The parameter h denotes a ratio between the explicit term and the implicit one in each of the equations; when h=0.5, the system of Eqs. (26)-(28) becomes the Crank-Nicolson scheme (Press et al., 1988). Thus, the discrete version of Eq. (1) becomes

$$-hD_{uy}u_{i,j-1}^{k+1} - hD_{ux}u_{i-1,j}^{k+1} + \left[1 + 2h(D_{ux} + D_{uy})\right]u_{i,j}^{k+1} - hD_{ux}u_{i+1,j}^{k+1} - hD_{uy}u_{i,j+1}^{k+1}$$
$$= (1-h)D_{uy}u_{i,j-1}^k + (1-h)D_{ux}u_{i-1,j}^k + \left[1 + 2(1-h)(D_{ux} + D_{uy})\right]u_{i,j}^k \tag{29}$$
$$+ (1-h)D_{ux}u_{i+1,j}^k + (1-h)D_{uy}u_{i,j+1}^k + \delta t f(u_{i,j}^k, v_{i,j}^k),$$

where

$$D_{ux} = D_u \delta t / \delta x^2, \ D_{uy} = D_u \delta t / \delta y^2. \tag{30}$$

By applying Eq. (29) to a particular point on an image, we obtain a set of linear equations. For example, the Gauss-Seidel method iteratively solves the set of equations (Press et al., 1988).

The previous study done by the authors and their collaborators implies that the choices of the spatial finite differences are very important, and it suggested that rather large finite differences would be better for the edge detection algorithm (Ebihara et al., 2003a).

5. Experimental Results

This section presents experimental results for the performance comparison of the reaction-diffusion algorithm and other competitive algorithms for edge detection, grouping and stereo disparity detection. Table 1 summarizes the algorithms, their parameter values utilized here and references to the results.

	Algorithm and model equation(s)	Parameter values	Results
Edge detection	Reaction-diffusion algorithm: Eqs. (17)-(19)	$\delta x = \delta y = 1/2$, $\delta t = 1/1000$, $D_u = 1.0$, $D_v = 5.0$, $D_a = 100$, $a_0 = 0.25$, $b = 1.0$, $\varepsilon = 10^{-3}$	Fig. 8
	DOG filter realized with two diffusion equations: Eq. (8)	$\delta x = \delta y = 1/2$, $\delta t = 1/1000$, $D_u = 1.0$, $D_v = 2.56$	
Grouping	Reaction-diffusion algorithm: Eqs. (21)-(24)	$\delta x = \delta y = 1/10$, $\delta t = 1/1000$, $D_u = 1.0$, $D_v = 3.0$ or 1.0, $a_0 = 0.15$, $b = 10$, $\varepsilon = 10^{-2}$, $\mu = 100$	Figs. 9,10 Table 2
	Single diffusion algorithm: Eqs. (21), (24) with $f(u_n, v_n, U_n) = 0$	$\delta x = \delta y = 1/10$, $\delta t = 1/1000$, $D_u = 1.0$, $\mu = 100$	
Stereo disparity detection	Reaction-diffusion algorithm: Eqs. (21), (22), (24), (25)	$\delta x = \delta y = 1/5$, $\delta t = 1/100$, $D_u = 1.0$, $D_v = 3.0$, $a_0 = 0.13$, $a_1 = 1.5$, $b = 10$, $\varepsilon = 10^{-2}$, $\mu = 3.0$	Figs. 11-13 Table 3
	Cooperative algorithm: Eqs. (14)-(16)	$\alpha = 2.0$, $T = 0$, $\Omega_e = 5 \times 5 \times 3$, $C_d = 0.08$ if $C_d < 0.08$	

Table 1. Algorithms, their parameter values utilized in the experiments and references to the figures and tables showing their results. The ratio h needed for the finite difference method was fixed at $h = 0.5$. For stereo disparity detection, both the reaction-diffusion algorithm and the cooperative algorithm utilize a cross-correlation map $C_d(x,y)$ evaluated by Eq. (10), in which the spatial local area L_S consists of the target point and its 4 nearest points, that is, $L_S = \{(x,y) \mid (0,0),(1,0),(0,1),(-1,0),(0,-1)\}$. Neither of the stereo algorithms has sub-pixel accuracy on disparity. The authors realized the computer programs of all the algorithms including the competitive ones by themselves.

5.1 Edge detection

Figure 8 shows edge detection results obtained for an image of the outdoor scene shown in Fig. 8(a). Figure 8(b) shows the distribution $u(x,y,t=10)$ obtained by the reaction-diffusion algorithm; this distribution directly expresses edge points. Figure 8(c) shows the difference of the two solutions u and v governed by the two diffusion equations having small and large diffusion coefficients ($D_u < D_v$); the difference corresponds to that of the DOG filter proposed by Marr and Hildreth [see Eq. (8) and section 3]. The zero-crossing points in Fig. 8(c) correspond to the edge points as shown in Fig. 8(d). The reaction-diffusion algorithm detects and preserves sharp corners, in contrast to the DOG filter. This is the main feature of the reaction-diffusion algorithm applied to edge detection.

(a)   (b)

(c)   (d)
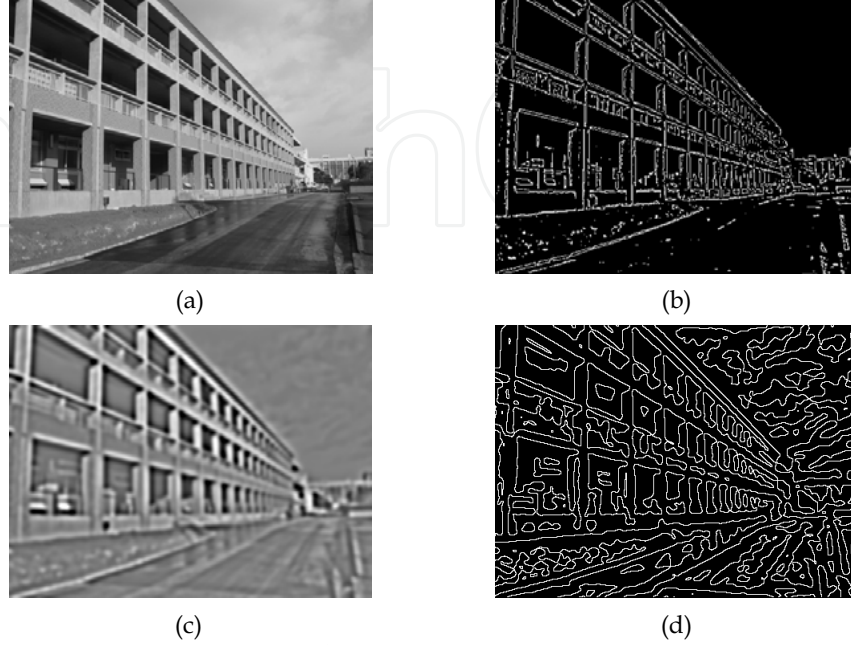
Figure 8. Results of edge detection for a real image. (a) Original image, 450×340 pixels and 256 brightness levels. (b) Solution $u(x,y,t=10)$ obtained by the reaction-diffusion algorithm. (c) Difference of two solutions $[u(x,y,t=1.0)-v(x,y,t=1.0)]$ in Eq. (8). (d) Zero-crossing points obtained from (c). White lines and dots correspond to edge points in (b) and (d). See Table 1 for the algorithms and parameter values utilized here.

5.2 Grouping

The reaction-diffusion algorithm and its competitive single diffusion algorithm were applied to the filter outputs in Fig. 7 derived from Fig. 5(b). Figure 9(a) shows the result of the reaction-diffusion algorithm having the large inhibitory diffusion coefficient D_v=3.0; Fig. 9(b) shows the result with D_v=1.0 being equal to D_u. For comparison, Fig. 9(c) shows the result obtained by the single diffusion algorithm, which is derived from the reaction-diffusion algorithm with $f(u_n,v_n,U_n)$=0 in Eq. (21). The next error measure evaluates the difference between the true group map $M_t(x,y)$ and an obtained one $M_c(x,y,t)$:

$$E(t) = \frac{1}{N_F} \sum_{(x,y)\in F} \sigma\big(\big|M_t(x,y) - M_c(x,y,t)\big|, 1.0\big) \times 100 \quad (\%) \tag{31}$$

The set F contains all of the points on an image plane, and N_F is the number of points in F. Figure 10 and Table 2 show the results of error evaluation for the algorithms. These results show the similar minimum errors (Table 2). The single diffusion algorithm achieves the minimum error at t=0.4; however, after that, the error is rapidly increasing monotonically. The reaction-diffusion algorithm with D_v=3.0 achieves the best evaluation of the minimum error at t=1.6. After that, the error is slightly increasing and finally it converges with good evaluation. The result using the reaction-diffusion algorithm with D_v=3.0 is better than that with D_v=1.0.
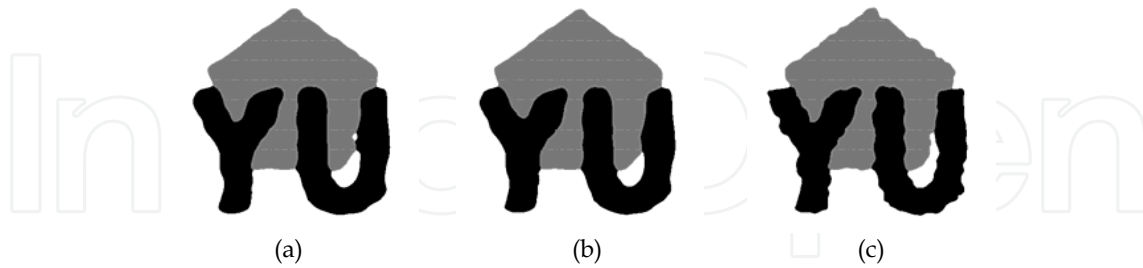
(a)   (b)   (c)

Figure 9. Results of grouping obtained by the reaction-diffusion algorithm with (a) D_v=3.0 at t=1.6, (b) D_v=1.0 at t=1.1 and (c) by the single diffusion algorithm at t=0.4. See Table 1 for the algorithms and parameter values utilized here. Figure 5 shows the original image of the visual stimulus, and Fig. 7 shows the outputs of orientation-selective filters.
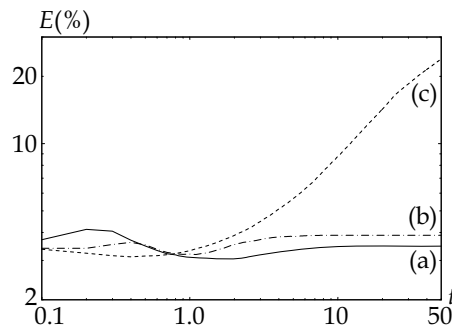

Figure 10. Temporal error changes evaluated for the results of the grouping process by the error measure $E(t)$ of Eq. (31). (a) Reaction-diffusion algorithm with D_v=3.0; (b) reaction-diffusion algorithm with D_v=1.0; (c) single diffusion algorithm. See Table 1 for the algorithms and parameter values. See Fig. 9 for the group maps at the minimum error.

Algorithm	Reaction-diffusion algorithm		Single diffusion algorithm
	D_v=3.0	D_v=1.0	
Minimum error	$E(t$=1.6)=3.05 (%)	$E(t$=1.1)=3.19 (%)	$E(t$=0.4)=3.12 (%)
Final error	$E(t$=50) =3.48 (%)	$E(t$=50) =3.89 (%)	$E(t$=50) =23.9 (%)

Table 2. Error comparison among the results of the reaction-diffusion algorithm and the single diffusion algorithm by the error measure $E(t)$ of Eq. (31). See Table 1 for the algorithms and their parameter values and Fig. 9 for the group maps at the minimum error.

5.3 Stereo disparity detection

The reaction-diffusion algorithm and the previous cooperative algorithm proposed by Zitnick and Kanade were applied to the well-known stereo images of TSUKUBA and VENUS for performance evaluation of stereo algorithms. Both the image pairs and their true disparity maps are available via the website http://www.middlebury.edu/stereo. Figures 11 and 12 show the stereo images, the true disparity map, a cross-correlation map and disparity maps obtained by the two algorithms.

Two kinds of error measures, E_{RMS} and E_{BMP} (Scharstein and Szeliski, 2002) evaluate the obtained disparity maps. The error measure E_{RMS} evaluates the root-mean-square error for an obtained stereo disparity map, as follows:

$$E_{\mathrm{RMS}}(t) = \left\{ \frac{1}{N_{F_{\neg O}}} \sum_{(x,y) \in F_{\neg O}} [M_t(x,y) - M_c(x,y,t)]^2 \right\}^{1/2} . \qquad (32)$$

The set $F_{\neg O}$ contains all of the points detected on an image plane except for the occlusion area and border; $N_{F_{\neg O}}$ is the number of points in $F_{\neg O}$. Thus, the error measure evaluates how much an obtained disparity map $M_c(x,y,t)$ differs from the true one $M_t(x,y)$. The error measure E_{BMP} evaluates the ratio of the number of correct match points to that of detected points $N_{F_{\neg O}}$, as follows:

$$E_{\mathrm{BMP}}(t) = \frac{1}{N_{F_{\neg O}}} \sum_{(x,y) \in F_{\neg O}} \sigma \left(\left| M_t(x,y) - M_c(x,y,t) \right|, \delta d \right) \times 100 \quad (\%). \qquad (33)$$

The parameter δd denotes the threshold value for the judgement of bad match or a correct one; it was fixed at $\delta d = 1.0$ pixel throughout the present experiments.
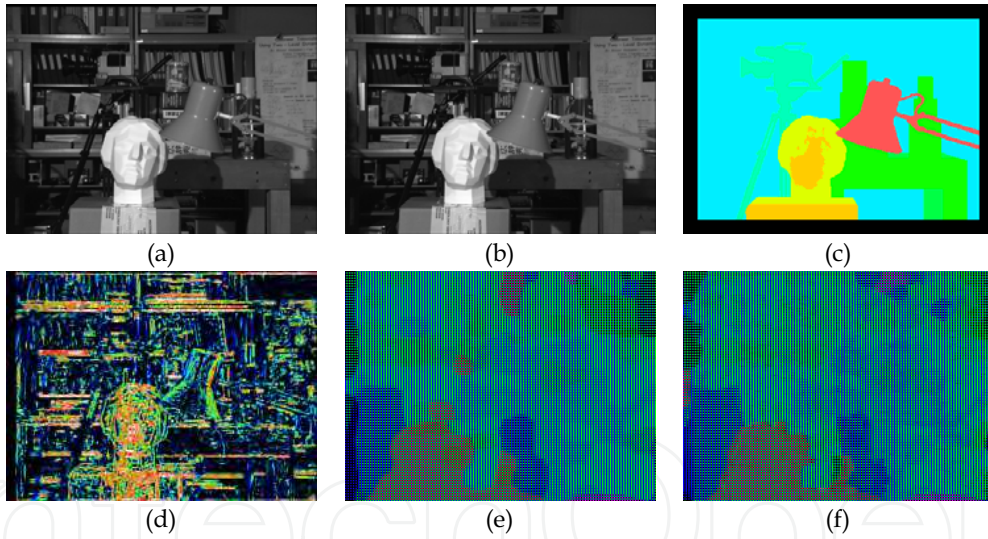

Figure 11. Stereo disparity detection for the image pair of TSUKUBA. (a) Left and (b) right images and (c) true disparity map $M_t(x,y)$. The image size is 384×288 pixels, and possible disparity levels are $\Psi_d = \{0,1,\ldots,15\}$ pixels. (d) Cross-correlation map $C_d(x,y)$ at the disparity level $d=11$ pixels. Disparity maps $M_c(x,y,t)$ obtained by (e) the reaction-diffusion algorithm at $t=50$ and (f) the cooperative algorithm at $t=100$. See Table 1 for the algorithms and parameter values utilized here. The stereo image pair is available via the website http://www.middlebury.edu/stereo (Scharstein and Szeliski, 2002).
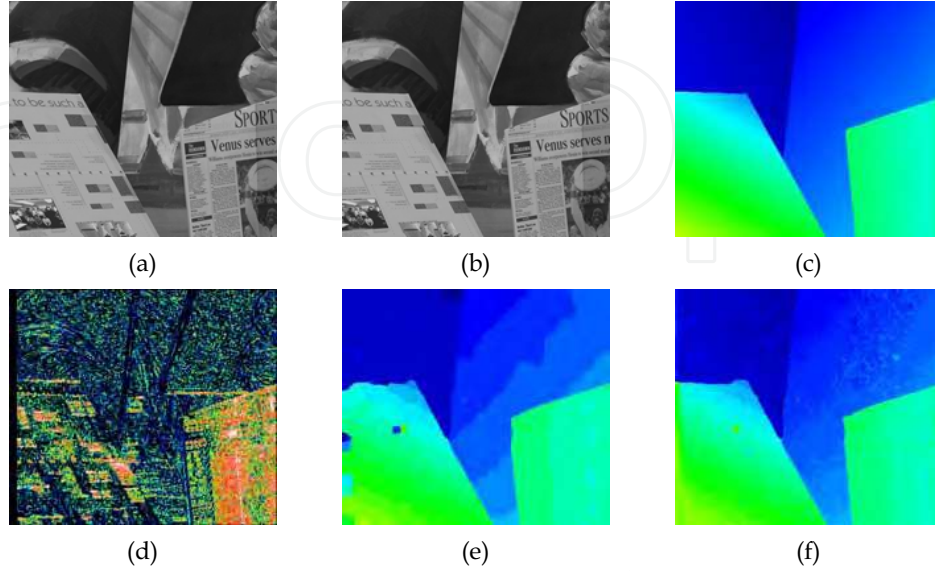
Figure 12. Stereo disparity detection for the image pair of VENUS. (a) Left and (b) right images and (c) true disparity map $M_t(x,y)$. The image size is 434×383 pixels, and possible disparity levels are Ψ_d={0,1,···,19} pixels. (d) Cross-correlation map $C_d(x,y)$ obtained at the disparity level d=12 pixels. Disparity maps $M_c(x,y,t)$ obtained by (e) the reaction-diffusion algorithm at t=50 and (f) the cooperative algorithm at t=100. See Table 1 for the algorithms and parameter values utilized here. The stereo image pair is available via the website http://www.middlebury.edu/stereo (Scharstein and Szeliski, 2002).
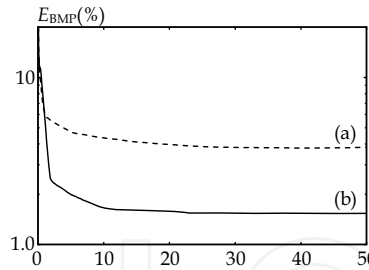
Figure 13. Temporal error changes evaluated for the disparity maps obtained by the reaction-diffusion algorithm. The bad-match-percentage error measure E_{BMP} of Eq. (33) was applied to the disparity maps detected from (a) TSUKUBA (Fig. 11) and (b) VENUS (Fig. 12).

Algorithm	Reaction-diffusion algorithm		Cooperative algorithm	
TSUKUBA	E_{RMS}=1.23 (pixel)	E_{BMP}=3.89 (%)	E_{RMS}=1.09 (pixel)	E_{BMP}=3.60 (%)
VENUS	E_{RMS}=0.677 (pixel)	E_{BMP}=1.54 (%)	E_{RMS}=0.691 (pixel)	E_{BMP}=4.32 (%)

Table 3. Performance comparison between the reaction-diffusion algorithm and the previous cooperative algorithm for the stereo image pairs of TSUKUBA and VENUS. See Table 1 for the algorithms and parameter values, and Figs. 11 and 12 for the disparity maps. See Eq. (32) for the error measure E_{RMS} and Eq. (33) for E_{BMP}.

Figure 13 shows the temporal changes of the bad-match-percentage error measure E_{BMP} for the results of the reaction-diffusion algorithm. The temporal changes show the convergence of the reaction-diffusion algorithm. In addition, for quantitative comparison, Table 3 shows the error measures evaluated for the results of the two algorithms. From these results, we see that the reaction-diffusion algorithm achieves good performance in the detection of stereo disparity.

6. Conclusion

This chapter presented the reaction-diffusion algorithm for vision systems. After a brief explanation of the reaction-diffusion system, we presented a class of algorithms for edge detection, grouping and stereo disparity detection by utilizing the FitzHugh-Nagumo type reaction-diffusion equations; all of the algorithms are necessary for the realization of vision systems. Previous algorithms, in particular, those proposed by Marr and his collaborators, utilize the Gaussian filter; the output of the filter is equivalent to the solution of the diffusion equation. In contrast to this, the reaction-diffusion algorithm has non-linear reaction terms coupled with diffusion equations. The non-linearity of the algorithm and the Turing-like condition can help to achieve good performance in edge detection, grouping and stereo disparity detection. Recently, the authors found a key mechanism in the stochastic resonance for performance improvement (Ebihara et al., 2003b). Thus, we conclude this chapter by noticing that further performance improvement will be possible with the use of the stochastic resonance in the reaction-diffusion algorithm.

7. References

Adamatzky, A.; Costello, B. D. L. & Asai, T. (2005). *Reaction-Diffusion Computers*, Elsevier, Amsterdam

Asai, T.; Costello, B. D. L. & Adamatzky, A. (2005). Silicon implementation of a chemical reaction-diffusion processor for computation of Voronoi diagram. *International Journal of Bifurcation and Chaos*, Vol. 15, pp. 3307-3320

Beck, J. (1966). Effect of orientation and of shape similarity on perceptual grouping. *Perception & Psychophysics*, Vol. 1, pp. 300-302

Brown, M. Z.; Burschka, D. & Hager, G. D. (2003). Advances in computational stereo. *IEEE Transactions on Pattern Analysis and Machine Intelligence*, Vol. 25, pp. 993-1008

Ebihara, M.; Mahara, H.; Sakurai, T.; Nomura, A. & Miike, H. (2003a). Image processing by a discrete reaction-diffusion system, *Proceedings of the 3rd IASTED International Conference on Visualization, Imaging, and Image Processing*, pp. 448-453, Benalmádena, Spain, September 2003

Ebihara, M.; Mahara, H.; Sakurai, T.; Nomura, A.; Osa, A. & Miike, H. (2003b). Segmentation and edge detection of noisy image and low contrast image based on a reaction-diffusion model. *The Journal of the Institute of Image Electronics Engineers of Japan*, Vol. 32, pp. 378–385 [in Japanese]

FitzHugh, R. (1961). Impulses and physiological states in theoretical models of nerve membrane. *Biophysical Journal*, Vol. 1, pp. 445-466

Gonzalez, R. C. & Woods, R. E. (1992). *Digital Image Processing*, Addison-Wesley Publishing Company, Reading

Julesz, B. (1960). Binocular depth perception of computer-generated patterns. *The Bell System Technical Journal*, Vol. 39, pp. 1125-1162

Kondo, S. & Asai, R. (1995). A reaction-diffusion wave on the skin of the marine angelfish *Pomacanthus*. *Nature*, Vol. 376, pp. 765-768

Kuhnert, L. (1986). A new optical photochemical memory device in a light-sensitive chemical active medium. *Nature*, Vol. 319, pp. 393-394

Kuhnert, L.; Agladze, K. I. & Krinsky, V. I. (1989). Image processing using light-sensitive chemical waves. *Nature*, Vol. 337, pp. 244-247

Marr, D. & Poggio, T. (1976). Cooperative computation of stereo disparity. *Science*, Vol. 194, pp. 283-287

Marr, D.; Palm, G. & Poggio, T. (1978). Analysis of a cooperative stereo algorithm. *Biological Cybernetics*, Vol. 28, pp. 223-239

Marr, D. & Hildreth, E. (1980). Theory of edge detection. *Proceedings of the Royal Society of London. Series B, Biological Sciences*, Vol. 207, pp. 187-217

Marr, D. (1982). *Vision*, W. H. Freeman and Company, New York

Murray, J. D. (1989). *Mathematical Biology*, Springer-Verlag, Berlin

Nagumo, J.; Arimoto, S. & Yoshizawa, S. (1962). An active pulse transmission line simulating nerve axon. *Proceedings of the I.R.E.*, Vol. 50, pp. 2061-2070

Nomura, A.; Ichikawa, M. & Miike, H. (1999). Solving random-dot stereograms with a reaction-diffusion model under the Turing instability, *Proceedings of the 10th International DAAAM Symposium*, pp. 385-386, Wien, Austria, October 1999

Nomura, A.; Ichikawa, M.; Miike, H.; Ebihara, M.; Mahara, H. & Sakurai, T. (2003). Realizing visual functions with the reaction-diffusion mechanism. *Journal of the Physical Society of Japan*, Vol. 72, pp. 2385-2395

Nomura, A.; Ichikawa, M. & Miike, H. (2004). Realizing the grouping process with the reaction-diffusion model. *IPSJ Transactions on Computer Vision and Image Media*, Vol. 45 (SIG 8/CVIM-9), pp. 26–39 [in Japanese]

Nomura, A.; Ichikawa, M. & Miike, H. (2005). Stereo vision system with the grouping process of multiple reaction-diffusion models. *Lecture Notes in Computer Science* 3522, Part I, pp. 137-144

Perona, P. & Malik, J. (1990). Scale-space and edge detection using anisotropic diffusion. *IEEE Transactions on Pattern Analysis and Machine Intelligence*, Vol. 12, pp. 629-639

Press, W. H.; Teukolsky, S. A.; Vetterling, W. T. & Flannery, B. P. (1988). *Numerical Recipes in C*, Cambridge University Press, Cambridge

Scharstein, D. & Szeliski, R. (2002). A taxonomy and evaluation of dense two-frame stereo correspondence algorithms. *International Journal of Computer Vision*, Vol. 47, pp. 7-42

Sunayama, T.; Ikebe, M.; Asai, T. & Amemiya, Y. (2000). Cellular vMOS circuits performing edge detection with difference-of-Gaussian filters. *Japanese Journal of Applied Physics*, Vol. 39, pp. 2278-2286

Turing, A. M. (1952). The chemical basis of morphogenesis. *Philosophical Transactions of the Royal Society of London. Series B, Biological Sciences*, Vol. 237, pp. 37-72

Zitnick, C. L. & Kanade, T. (2000). A cooperative algorithm for stereo matching and occlusion detection. *IEEE Transactions on Pattern Analysis and Machine Intelligence*, Vol. 22, pp. 675-684

Vision Systems: Segmentation and Pattern Recognition

Edited by Goro Obinata and Ashish Dutta

Research in computer vision has exponentially increased in the last two decades due to the availability of cheap cameras and fast processors. This increase has also been accompanied by a blurring of the boundaries between the different applications of vision, making it truly interdisciplinary. In this book we have attempted to put together state-of-the-art research and developments in segmentation and pattern recognition. The first nine chapters on segmentation deal with advanced algorithms and models, and various applications of segmentation in robot path planning, human face tracking, etc. The later chapters are devoted to pattern recognition and covers diverse topics ranging from biological image analysis, remote sensing, text recognition, advanced filter design for data analysis, etc.

How to reference

In order to correctly reference this scholarly work, feel free to copy and paste the following:

Atsushi Nomura, Makoto Ichikawa, Rismon H. Sianipar and Hidetoshi Miike (2007). Reaction-Diffusion Algorithm for Vision Systems, Vision Systems: Segmentation and Pattern Recognition, Goro Obinata and Ashish Dutta (Ed.), ISBN: 978-3-902613-05-9, InTech, Available from: http://www.intechopen.com/books/vision_systems_segmentation_and_pattern_recognition/reaction-diffusion_algorithm_for_vision_systems

INTECH
open science | open minds